Mechanical property degradation of high crystalline SiC fiber–reinforced SiC matrix composite neutron irradiated to ~100 displacements per atom*

Takaaki Koyanagi[a†], Takashi Nozawa[b], Yutai Katoh[a], Lance L Snead[c]

[a]Oak Ridge National Laboratory, 1 Bethel Valley Road, Oak Ridge, TN 37831, United States

[b]National Institutes for Quantum and Radiological Science and Technology, 2-166 Omotedate, Obuchi, Rokkasho, Aomori 039-3212, Japan

[c]Stony Brook University, 100 Nicolls Rd, Stony Brook, NY 11794, United States

Abstract

For the development of silicon carbide (SiC) materials for next-generation nuclear structural applications, degradation of material properties under intense neutron irradiation is a critical feasibility issue. This study evaluated the mechanical properties and microstructure of a chemical vapor infiltrated SiC matrix composite, reinforced with a multi-layer SiC/pyrolytic carbon–coated Hi-Nicalon™ Type S SiC fiber, following neutron irradiation at 319 and 629°C to ~100 displacements per atom. Both the proportional limit stress and ultimate flexural strength were significantly degraded as a result of irradiation at both temperatures. After irradiation at 319°C, the quasi-ductile fracture behavior of the nonirradiated composite became brittle, a result that

† Corresponding author: Oak Ridge National Laboratory, 1 Bethel Valley Road, Oak Ridge, TN 37831-6140 USA, Email: koyanagit@ornl.gov, Tel: +1-865-574-8764

was explained by a loss of functionality of the fiber/matrix interface associated with the disappearance of the interphase due to irradiation. The specimens irradiated at 629°C showed increased apparent failure strain because the fiber/matrix interphase was weakened by irradiation-induced partial debonding.

Keywords

Silicon carbide, Ceramics matrix composite, Neutron irradiation, Mechanical properties

Introduction

Continuous silicon carbide (SiC) fiber–reinforced SiC matrix (SiC/SiC) composites are leading candidates for use as structural materials for advanced nuclear reactor components such as fusion blanket components [1-3], fuel cladding and channel boxes for light water reactors [4-6], and fuel cladding and control rods for gas-cooled fast reactors [7, 8]. They are of interest because of their inherent high dissociation temperatures, chemical stability [9], relatively low neutron absorption [10], high toughness [11], relatively mature fabrication technology [11, 12], and so on. To enable the successful development of SiC/SiC composites for advanced reactors, the effects of high-dose fusion or fission neutron irradiation on their mechanical and physical properties are critical phenomena that must be considered. The neutron doses for SiC/SiC components are expected to reach beyond 100 displacements per atoms (dpa), depending on the reactor design [13]. For example, SiC/SiC composite fuel cladding and core structures for gas-cooled fast reactors and SiC/SiC composite fusion reactor components are expected to receive intense neutron irradiation to ~100 dpa during their service lives [7]. Although the lifetime neutron dose SiC/SiC composites will receive is not specified for each application, it is possible

that the material degradation associated with high-dose irradiation will be a limiting factor for the use of SiC/SiC composite materials in radiation environments.

Very high-dose neutron irradiation of a β SiC monolith up to 1.9×10^{27} n/m^2 (E > 0.1 MeV) at 370–650°C was achieved in fast breeder reactors by Yano et al. [14-16]. They investigated irradiation-induced dislocation loops by transmission electron microscopy (TEM) and x-ray diffraction. They found growth of the dislocation loops with increasing neutron dose, although the growth was moderate; the average loop diameter was ~15 nm for the specimen irradiated to 1.0×10^{27} n/m^2 (E > 0.1 MeV). Moreover, a series of high-dose neutron irradiations was conducted at 300–800°C on a specific type of SiC/SiC composite: a chemical vapor infiltrated (CVI) SiC/SiC composite with Hi-Nicalon™ Type S (HNS) SiC fibers and a multi-layer pyrolytic carbon (PyC)/SiC interphase [17-20]. The important findings from these studies are (1) saturation swelling of the SiC/SiC composite up to ~70 dpa, (2) a saturation of degradation in the thermal diffusivity from a few dpa to ~70 dpa, and (3) irradiation-temperature–dependent degradation of flexural properties (resistant at higher radiation temperatures) beyond ~40 dpa. These results encouraged the use of SiC/SiC composites at higher irradiation temperatures and, at the same time, motivate further development of irradiation-resistant SiC/SiC composite materials for applications at relatively low irradiation temperatures. In this study, the series used in the high-dose irradiation study was extended to higher neutron doses of up to 105 dpa. The main objective of this study is to use microscopy analysis to understand the mechanism of degradation of the mechanical properties of irradiated SiC/SiC composites, which was not clearly identified in previous work [19, 20].

Experimental

The SiC/SiC material investigated was HNS fiber (lot number 2D2685-02-I5-01, year 2000) – reinforced CVI SiC/SiC composites fabricated by Hypertherm THC Inc. (now a subsidiary of Rolls Royce Inc.) The fiber architecture was a two-dimensional five-harness satin weave with a 0/90° stacking configuration. The fiber/matrix interphase was a five-layer ring-stack of ~10 nm thick PyC and ~100 nm thick SiC. This is a fiber/matrix interface design with a minimized thickness of the PyC phase [21]. The fiber volume fraction was approximately 35%. The mean density of the composite was 2.52 g/cm^3. The HNS fiber contained a carbon impurity phase, and the C/Si atomic ratio was 1.05 based on the material data sheet from the manufacturer. Also investigated was a monolithic chemical vapor deposited (CVD) SiC (CVD Silicon Carbide™ high-resistivity grade, Rohm and Haas Co.). The material purity was 99.9995%, as guaranteed by the vendor. The composite and monolithic materials were machined into flexural bars with dimensions of 50.8 (long) × 6.3 (wide) × 2.8 (thick) mm. For the composite, one of the fiber reinforcement directions was aligned to the specimen length direction. The direction of the fiber fabric stacks corresponded to the specimen thickness direction. More details of the specimen fabrication and preparation can be found elsewhere [17].

Neutron irradiation was conducted in the flux trap facility of the High Flux Isotope Reactor at Oak Ridge National Laboratory (ORNL). The nominal irradiation temperatures were ~300 and ~500 °C. The neutron dose was up to 105 dpa with an equibalance of 1 dpa = 1×10^{25} n/m^2 (E > 0.1 MeV) [17]. The total duration of the irradiation was 1000–1150 days. The irradiation conditions for the specimens are summarized in Table 1. Part of the specimen surfaces was contaminated during irradiation because of contact between the specimens and the metallic components of the irradiation vehicle. However, no significant reaction layer was found by observation, and the effect was minimal in a previous study using same irradiation capsule

design [20]. The actual irradiation temperatures were determined by the recovery behavior of the instantaneous coefficient of thermal expansion of a SiC passive thermometer made of CVD SiC, during annealing using a NETZSCH DIL 402CD horizontal dual pushrod dilatometer. The annealing was conducted at a heating rate of 1°C/min. and a cooling rate of 2.5°C/min. Details of the method of determining irradiation temperature were reported in [22]. The error in temperature determination by data analysis was typically 10–15°C [22]. Note that the specimens were designed to be irradiated in contact with the thermometer. The SiC passive temperature monitor provided the temperature at the end of irradiation. Because this study used the same irradiation vehicle design used in previous work, and the actual irradiation temperature of the previous specimens was close to the nominal temperature for doses of ~40 and ~70 dpa [20], the desired irradiation temperature was expected to be achieved if the temperature of the thermometer was reasonably close to the nominal temperature.

The dimensions of each specimen were obtained using a micrometer, which measured the length swelling at an accuracy of 0.05%. Swelling along the specimen width and thickness directions was not reported because of a significant deviation in the data. Mechanical properties of both the irradiated and the nonirradiated specimens were evaluated by four-point flexural testing at room temperature, according to ASTM C1341. The support span and the loading span were 40 and 20 mm, respectively. The proportional limit stress (PLS) was determined as a 5% deviation in stress from the initial linearity. The dynamic Young's moduli of the SiC/SiC composites were determined using the impulse excitation of vibration method in accordance with ASTM standard C1259, using an Integrated Material Control Engineering resonant frequency and damping analyzer. The fracture surfaces of the composites were characterized using a Hitachi 4800S

scanning electron microscope (SEM) for nonirradiated specimens and an FEI Quanta Dual Beam SEM/focused ion beam (FIB) for irradiated specimens.

As-irradiated specimens were also observed using a FEI Versa Dual Beam SEM/FIB. The TEM specimens were prepared using the FEI Versa Dual Beam SEM/FIB operated at 30 kV for rough milling and 2 and 5 kV for final thinning, followed by low-energy ion milling using a Fischione Model 1040 NanoMill operated at 600 and 900 eV. TEM observation was also conducted using a JEOL JEM2100F with TEM and scanning TEM (STEM) modes operated at 200 kV. STEM–electron energy loss spectroscopy (EELS) evaluation was conducted using a Gatan GIF Quantum post-column energy filter and Gatan Digital Micrograph software. The spectrometer correction angle was 4.2 mrad. Background removal of the EELS spectra was conducted using a Power Law fit model for carbon K-edge spectra. The TEM specimen thickness was determined by an EELS log-ratio method.

Table 1. Summary of irradiation conditions, dynamic Young's modulus, flexural properties, and swelling. Actual irradiation temperatures were determined using passive SiC thermometry. Parentheses indicate one standard deviation. Thirty nonirradiated specimens were tested in previous work [17]

Material	Design irradiation temperature [°C]	Actual irradiation temperature [°C]	Dose [dpa]	Specimen ID	Dynamic Young's modulus [GPa]	Transient modulus of elasticity [GPa]	PLS [MPa]	UFS [MPa]	Length swelling [%]
CVI SiC/SiC	Not applicable		0	Not available	228 (21)	179 (5)	395 (55)	453 (46)	0
CVI SiC/SiC	300	319	92	S06 S94	186 208	135 164	143 124	256 273	0.48 0.56
CVI SiC/SiC	500	629	99	S104 S110	187 219	142 168	225 206	256 273	0.38 0.35
CVD SiC	300	257	73	B42 B80	388 379	Not available			0.82 0.79

CVD SiC	500	534	105	B29 B38	Not available		0.64 0.63

Results

Mechanical properties and swelling

Flexural tests of nonirradiated specimens were conducted in the previous study [17]. This study used the same grade of material for irradiation and the same support/load span length for the flexural test. Fig. 1 shows the flexural behavior of nonirradiated and irradiated CVI SiC/SiC composites. The PLS and ultimate flexural strength (UFS) determined are listed in Table 1. The nonirradiated material shows typical fracture behavior for a tough composite, i.e., nonlinear fracture behavior beyond PLS. On the other hand, the specimen irradiated at 319°C to 92 dpa failed in a brittle manner; i.e., PLS was equal to UFS, and both PLS and UFS were significantly degraded. The specimen irradiated at 629°C to 99 dpa showed nonlinear fracture behavior with apparent increased failure strain. Complete failure could not be achieved because of contact between the fixture and the specimen under flexural strain beyond ~1%. In addition, the degradation of both PLS and UFS was obvious. These results are qualitatively similar for the specimens irradiated to ~70 dpa at similar temperatures [20].

Fig. 2 shows the dose dependence of PLS, UFS, dynamic Young's modulus, and swelling, together with the data obtained from previous studies using the same grade of material [17, 18, 20]. The graphs show the mechanical properties normalized by nonirradiated values. Degradation of both PLS and UFS started before 40 dpa at irradiation temperatures of 300–629°C. The SiC/SiC composite tended to possess higher PLS and UFS following irradiation at higher temperatures. The reduction of the Young's modulus of the SiC/SiC material ranged 5–20% in most cases and was insensitive to irradiation temperature. There was no progressive

length swelling from 40 to 100 dpa. In the CVD SiC monolith, the trends of reduction in the Young's modulus and length swelling were the same as in the composite material.

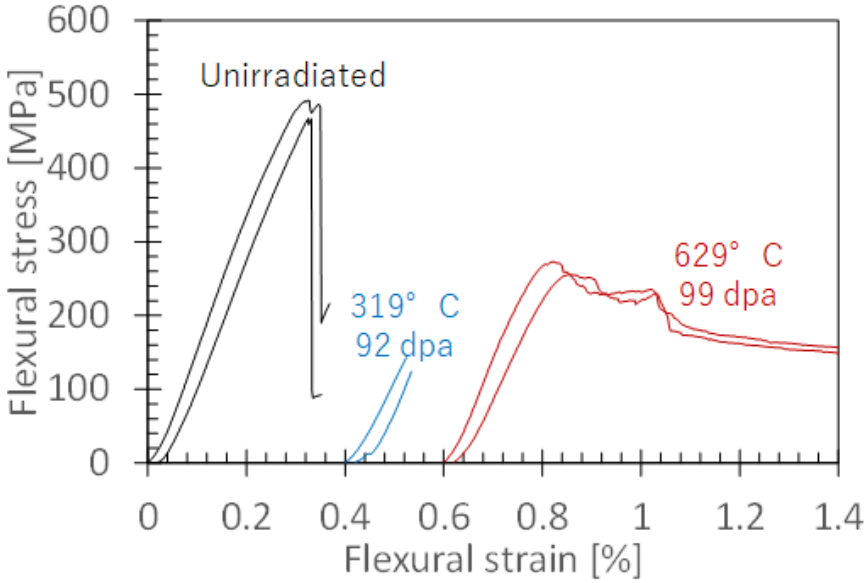

Fig. 1. Flexural behavior of nonirradiated and irradiated CVI SiC/SiC composites. The stress-strain curves are shifted to aid visibility.

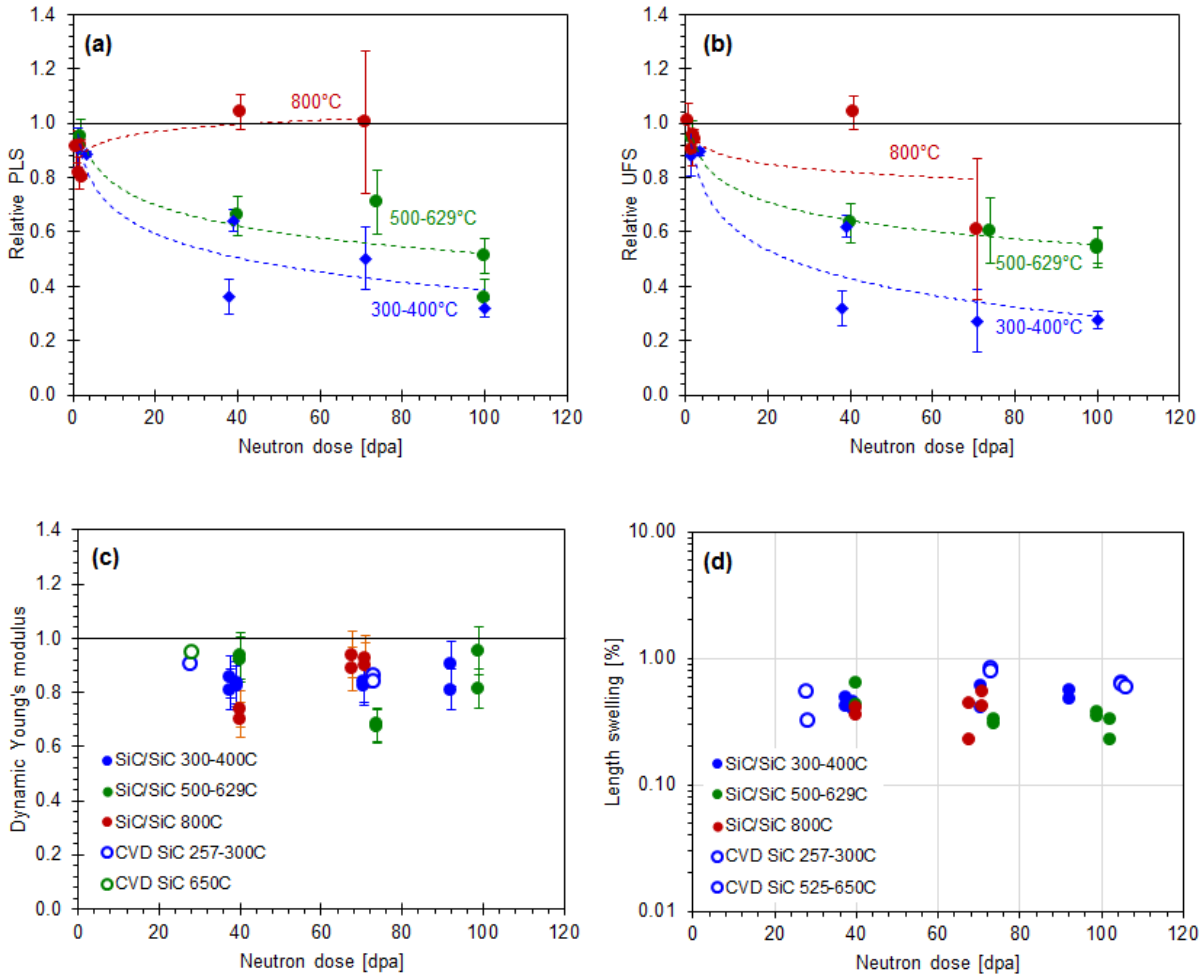

Fig. 2. Neutron dose dependence of (a) PLS, (b) UFS, (c) dynamic Young's modulus, and (d) length swelling of CVI SiC/SiC composite. The data for CVD SiC are also included for the dynamic Young's modulus and swelling. Some of these data were reported in previous work [17, 18, 20]. The broken lines in Fig (a) and (b) are fit by a logarithmic function to show the trend.

Microstructural analysis

Fig. 3 shows fractography results for the nonirradiated and irradiated SiC/SiC specimens, obtained using SEM. The nonirradiated specimens exhibited clear fiber pullout with typical lengths of below 100 μm. The fiber pullout explains the nonlinear fracture behavior of this

material [23] in Fig. 1. The fracture surface of the SiC/SiC composite irradiated at 319°C was relatively flat and almost no fiber pullout was observed, as expected from its brittle flexural behavior. Regarding the specimen irradiated at 629°C, fibrous failure was observed. The fiber pullout length was approximately 1 mm. The longer fiber pullout of this material compared with the pristine material is consistent with increased apparent failure strain due to irradiation, as observed in previous work [24]. The effects of irradiation were also found in the fracture appearance of the HNS fiber. While the nonirradiated fiber failed with rough fracture surfaces, the fracture surfaces following irradiation were relatively smooth. In the case of irradiation at 319°C, very smooth and flat fiber fracture surfaces were observed.

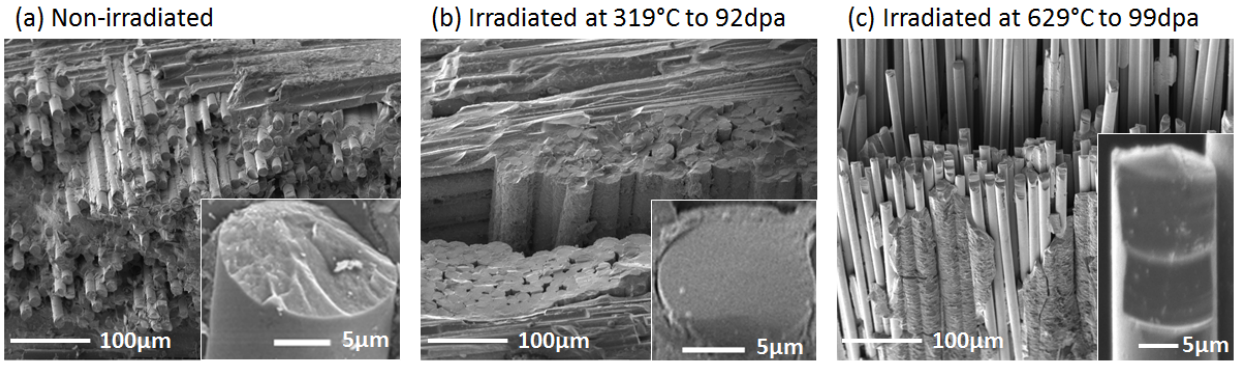

Fig. 3. Fracture appearance of nonirradiated and irradiated CVI SiC/SiC composites.

SEM observations of pristine and as-irradiated specimens were also conducted. As shown in Fig. 4a, the cross section of the specimen was prepared by conventional FIB milling. This method was used because mechanical polishing introduced damage, especially on the multi-layer interphase [19]. The secondary electron image of nonirradiated material (Fig. 4b) clearly shows five layers of PyC. Following irradiation at 319°C to 92 dpa, two irradiation-induced phenomena were found: partial debonding at the fiber/matrix interface and disappearance of the PyC contrast

(Fig. 4c). In the case of irradiation at 629°C to 99 dpa, it is clearly seen that small pores or defects formed within the PyC layer (Fig. 4d). The contrast of the PyC was recognized under these irradiation conditions. Crucially, these microstructural changes in the fiber/matrix interphase are related to flexural behaviors, as is discussed later in this paper.

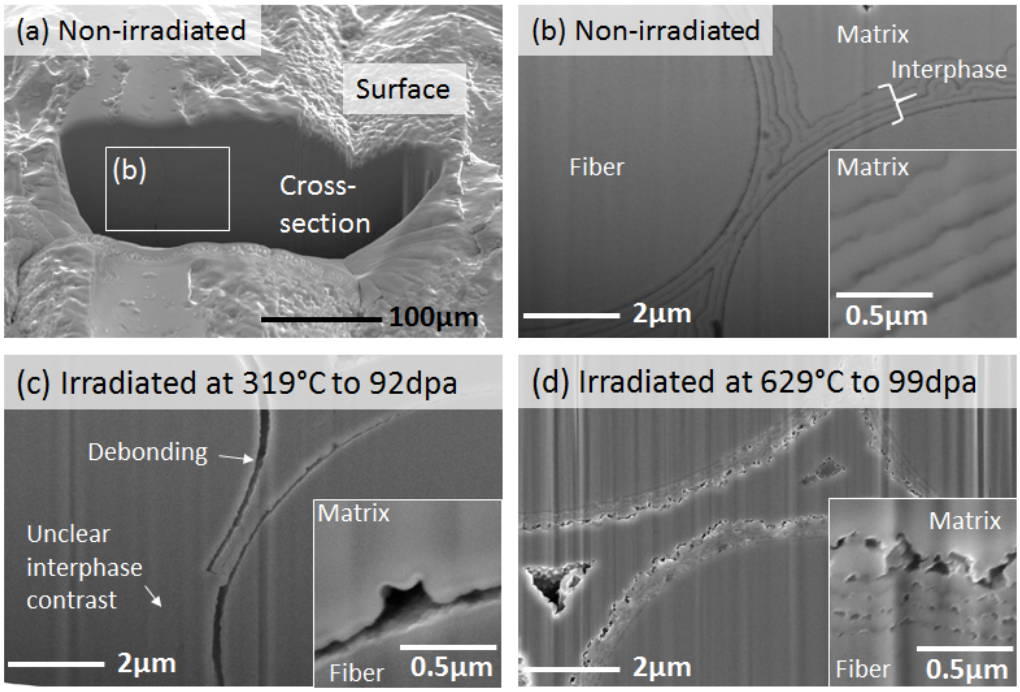

Fig. 4 Secondary electron micrographs of cross sections of CVI SiC/SiC composites: (a) cross section processed using FIB, (b) nonirradiated condition, (c) irradiated at 319°C to 92 dpa, and (d) irradiated at 629°C to 99 dpa. The observed area in the image is indicated in image (a)

The microstructures of the multi-layer interphase were also evaluated using TEM and STEM. The STEM high-angle annular dark field (HAADF) micrographs are shown in Fig. 5. The black contrast and brighter contrast indicate PyC and SiC phases, respectively. A layer of PyC ~10 nm

thick was observed in the pristine interphase. Irradiation at 319°C caused the partial disappearance of the PyC phase. The PyC phase irradiated at 629°C appeared to be preserved. Overall, the STEM-HAADF results are consistent with the SEM observations.

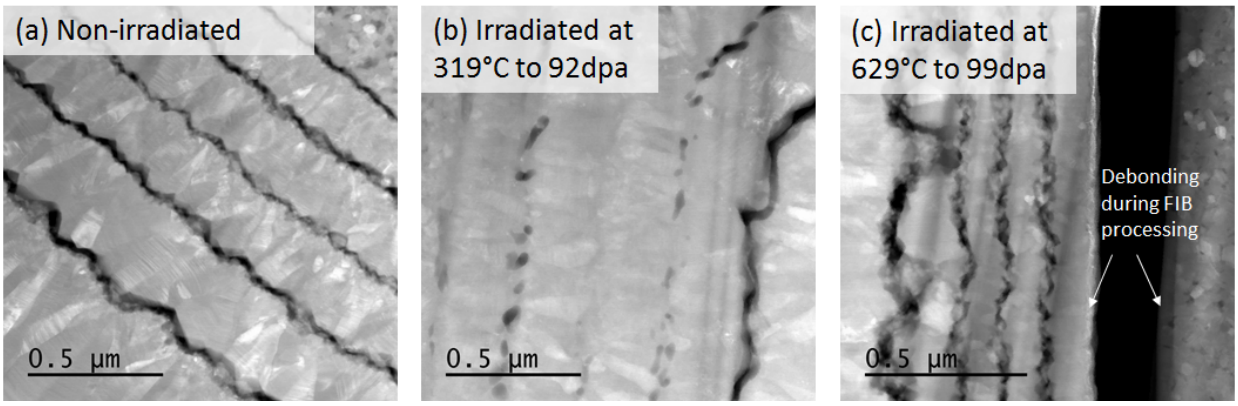

Fig. 5 STEM-HAADF images of PyC/SiC multi-layer interphase: (a) nonirradiated, (b) irradiated at 319°C to 92 dpa, and (c) irradiated at 629°C to 99 dpa.

The microstructure of PyC was closely observed by high-resolution TEM, as shown in Fig. 6. The nonirradiated PyC possessed a discontinuous stacking of graphene-like layers, which was also reported in Perez-Bergquist et al. and Kondo [19, 25]. This feature was completely lost following neutron irradiation at both 319 and 629°C. Detailed chemical analysis of the PyC phase was conducted by STEM-EELS point analysis. The EELS spectra were acquired with a spot size of 1.5 nm at the middle of the PyC width. The spectra of the specimen irradiated at 319°C were taken from the area where PyC was seen to remain in HAADF image. Fig. 7a and b show the energy loss spectra of the silicon L edge and carbon K edge, respectively. Only the carbon K edge peaks were detected in the nonirradiated PyC as normal. However, additional silicon L edge peaks were detected in the PyC irradiated at both 319 and 629°C. The signal was more evident for irradiation at 319°C. A peak was found at ~109 eV for 319°C and was broad for

629°C. These results are evidence of different bonding conditions of silicon atoms in the PyC phase. The energy-loss near-edge fine structure (ELNES) of the silicon L edge has a peak at ~105 eV for Si-C_3 (sp^3) bonding and no peak for Si-C_4 (sp^2d) bonding [26]. In addition, depending on the bonding condition, a peak shift of the ELNES of silicon was reported [26]. Effects of irradiation on the ELNES of the carbon K edge were also found. The nonirradiated spectrum had two characteristic features of the $1s \rightarrow \pi^*$ transition peak at ~285 eV and the weak $1s \rightarrow \sigma^*$ transition peak occurring at ~291 eV. The $1s \rightarrow \pi^*$ and $1s \rightarrow \sigma^*$ transition peaks are known to correspond to sp^2 and sp^3 hybridized carbon atoms, respectively. Irradiation at both 319 and 629°C resulted in the loss of the $1s \rightarrow \pi^*$ transition peak. Since the graphene structure was formed by sp^2 hybridized carbon atoms, the changes in the ELNES of the carbon K edge due to irradiation are consistent with the loss of layers of the graphene-like structure in Fig. 6. The effects of the EELS analysis on the ELNES of the carbon K edge are consistent with those in the previous ion irradiation study [25].

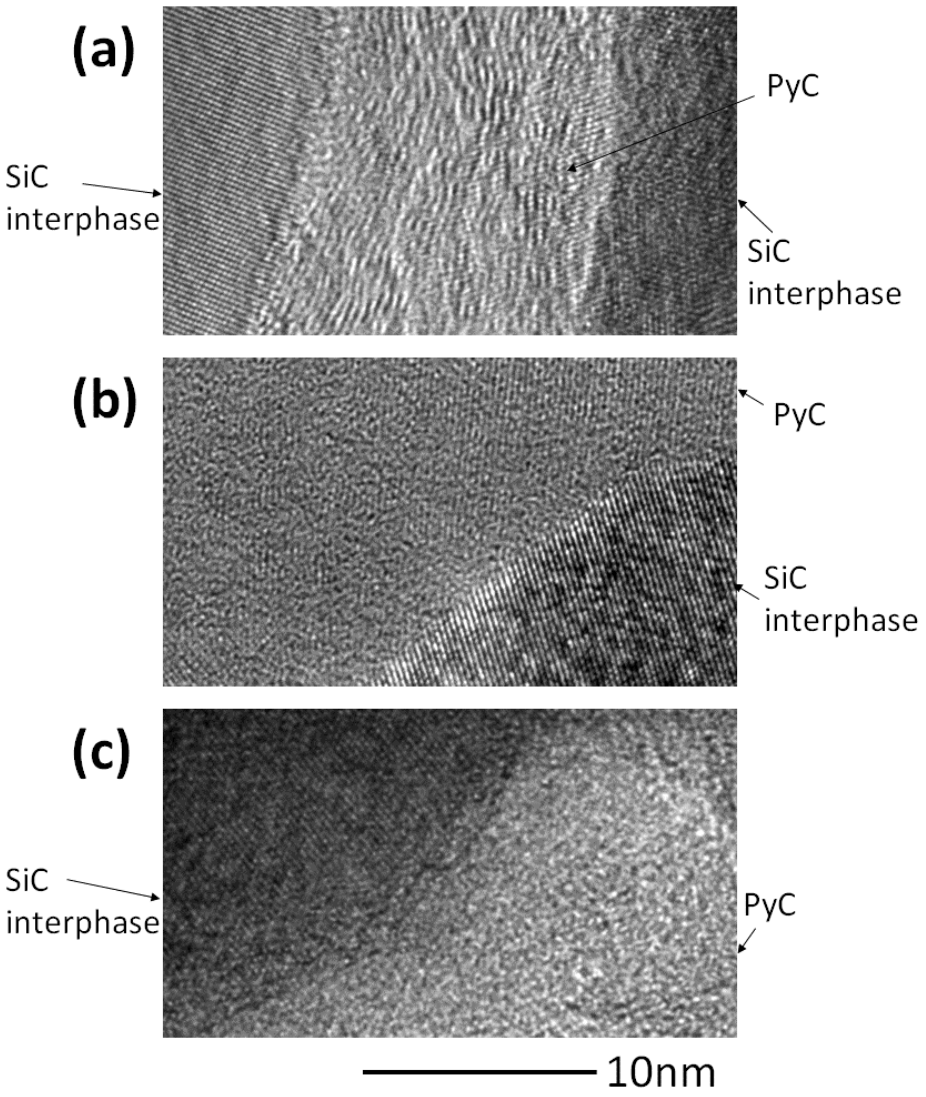

Fig. 6 High-resolution TEM micrographs of PyC/SiC multi-layer interphase: (a) nonirradiated, (b) irradiated at 319°C to 92 dpa, and (c) irradiated at 629°C to 99 dpa.

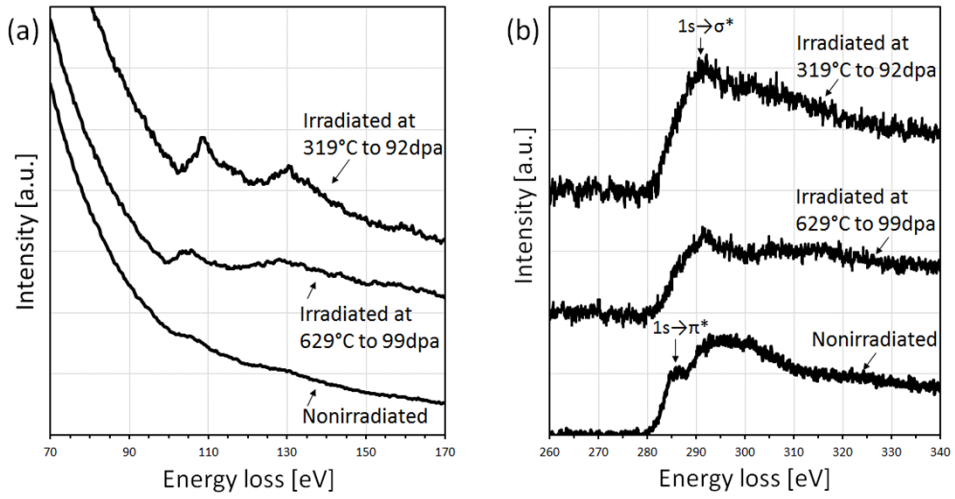

Fig. 7 Representative STEM-EELS spectrum of nonirradiated and irradiated PyC phase: (a) silicon L edge and (b) carbon K edge. The background of the spectra (a) is intended to remain to show the presence or absence of the energy loss from silicon atoms.

Microstructure of the HNS fibers were characterized by STEM-HAADF imaging. All the images in Fig. 8 were taken from near the fiber core. The black contrast shows carbon impurity phases, and the brighter contrast indicates SiC grains. The carbon impurity phase in HNS fiber was also reported in previous studies [19, 25]. It is obvious that the distribution of the carbon phases underwent modification by irradiation. The carbon phases were finely distributed at grain pockets in the nonirradiated condition. However, the number of carbon pockets was obviously reduced by irradiation; the number density of the carbon phases in the pristine fiber was ~8.5×10^{21} m^{-3}, and that was approximately halved by irradiation at both 319 and 629 °C. This phenomenon was also observed following neutron irradiation at 70 dpa [19] and self-ion irradiation at 300°C [25].

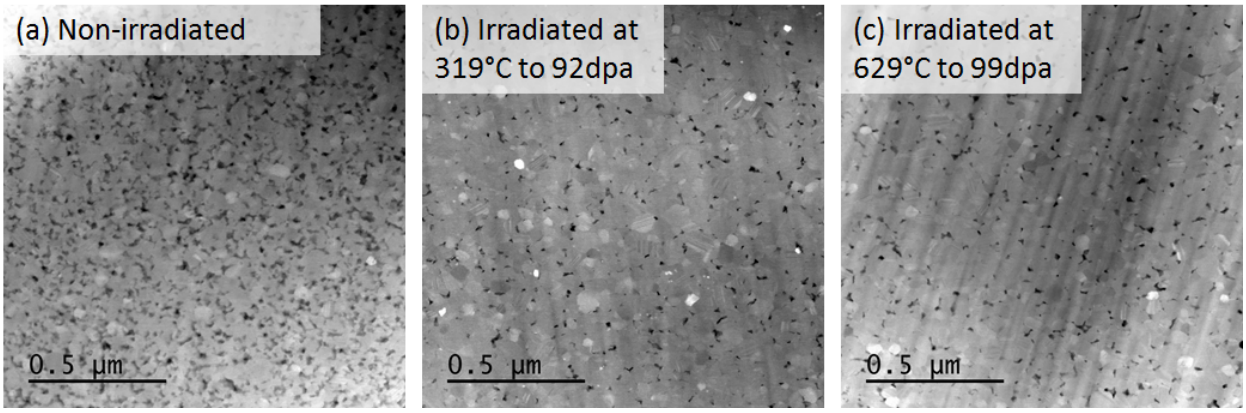

Fig. 8 STEM-HAADF micrographs of nonirradiated and irradiated HNS fibers.

Microstructures of the matrices of the CVI SiC/SiC composite and monolithic CVD SiC were also observed. The major microstructural difference among them in the as-fabricated condition is the presence of high-density stacking faults produced during processing of the CVI SiC/SiC matrix. The TEM observation found cavity formation within the composite matrix following irradiation at 629°C, via through-focus imaging (Fig. 9a, b), but did not find it at 319°C. Similar to the CVI SiC/SiC matrix, the cavities were observed in CVD SiC along the grain boundaries and the stacking faults following irradiation at 534°C. For both cases, the average cavity diameter and number density were ~2 nm and ~5×10^{22} m^{-3}, respectively, which corresponds to void swelling of only ~0.01 %. The void swelling was significantly less than the macroscopic volume swelling of 1.8%, indicating that point detects, small defect clusters, and dislocation loops mainly contributed to swelling. Irradiation-induced dislocations were also found in the irradiated CVD SiC. Bright-field TEM observation from near the [011] zone axis found the presence of edge-on dislocation loops on the {111} planes following irradiation at 257°C to 73 dpa and at 534°C to 105 dpa. This finding is consistent with previous work by Yano et al. [14]. The average dislocation diameter and number density of the loops on all {111} planes were

23 nm and 6.7×10^{22} m^{-3} for irradiation at 257°C, and 30 nm and 3.1×10^{22} m^{-3} at 534°C. Further identification of the nature of the dislocation loop is beyond the focus of this study. Note that this dislocation loop was not clearly observed in the CVI SiC/SiC matrix because of the difficulty of observing matrices with significant amounts of stacking faults as processing defects.

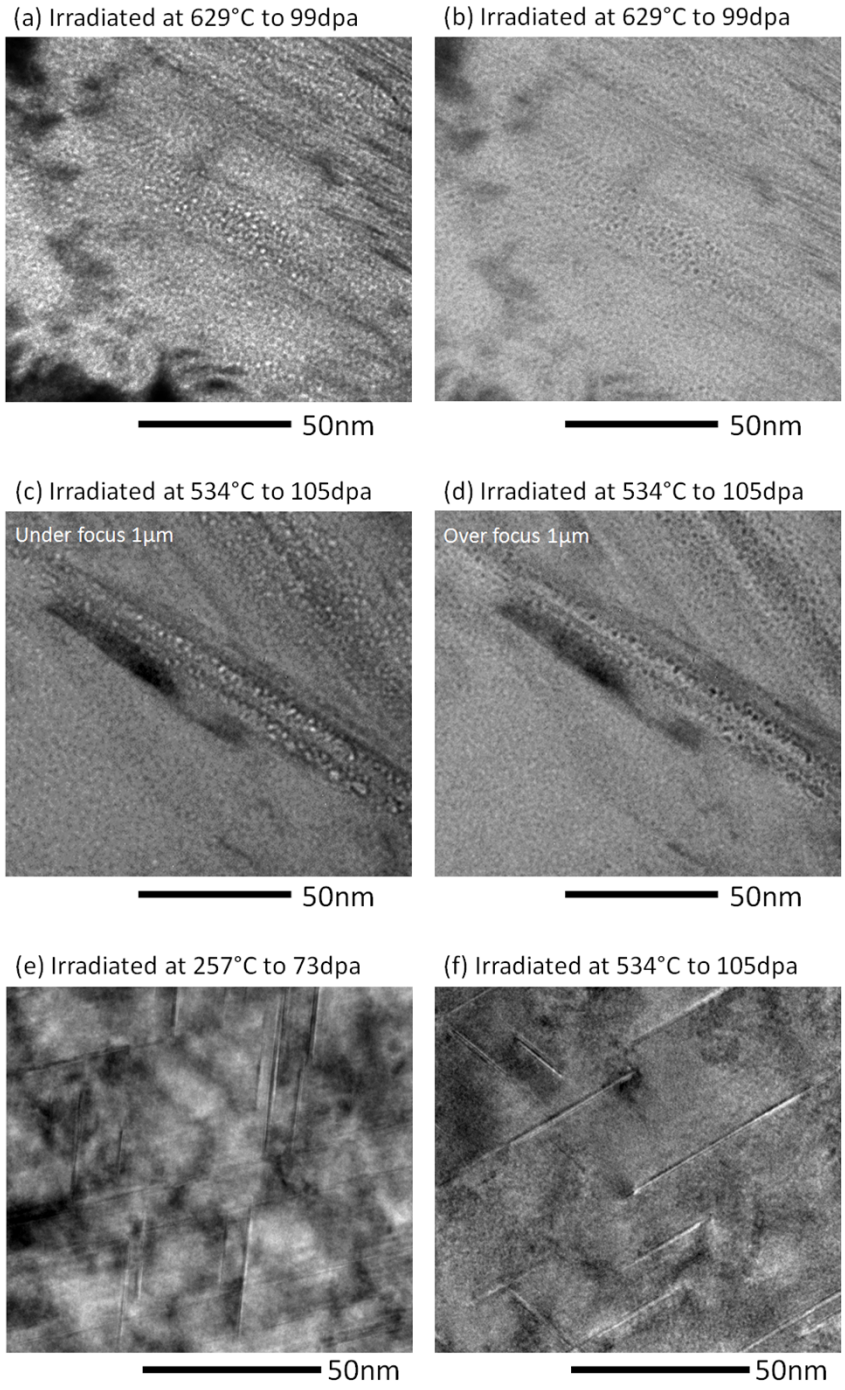

Fig. 9 Bright field TEM images of neutron-irradiated CVI SiC/SiC composite and monolithic CVD SiC: (a, b) cavity formation in matrix of CVI SIC/SiC composite, (c, d) cavity formation in CVD SiC, and (e, f) bright-field TEM image of CVD SiC taken from near [011] zone axis.

Discussion

The main focus of the discussion is the underlying mechanism of degradation of flexural behavior in irradiated SiC/SiC composites. Similar types of failure behavior (brittle failure at 300°C and increased failure strain at 500°C) were also found in a previous study of irradiation to ~70 dpa, which explained the mechanical degradation by fiber and/or interphase "damage" [20]. The current study identified the type of interphase damage using SEM (Fig. 4), and it importantly explains the fracture behavior. Under irradiation at 319°C, HNS fibers were partially debonded, and the remaining part was strongly bonded in part because of the disappearance of the PyC contrast seen in the STEM HAADF micrograph (Fig. 5). Given such a strong fiber/matrix bonding, it is expected that a composite toughening mechanism such as fiber pullout associated with the fiber/matrix friction [23] would not work because the bonded matrix and fiber would fail at the same time. This explains the brittle fracture behavior and flat fracture surface for this irradiation condition. In addition, the debonded location can be a failure initiation site and then degrade the PLS.

In the case of irradiation at 629°C, the PyC phase had a lot of small pores or local debonding spots that indicate weakened fiber/matrix interfacial bonding strength. This is consistent with the observed long fiber pullout and the increased apparent failure strain. Such weakened interfacial bonding between fiber and matrix and long fiber pullout were also reported in CVI SiC/SiC composites with monolayer PyC-coated Nicalon SiC fibers neutron irradiated at 300°C to 1 dpa

[24]. In theory, the weak fiber/matrix bonding also explains the degradation of the PLS—i.e., stress proceeding to critical matrix cracking—under monotonic tensile loading [27, 28]. For this irradiation condition, the apparent failure strain was increased but the UFS was degraded. This indicates a reduction in the fiber/matrix interfacial dissipation during loading, so that the applied stress is not effectively transferred to the fiber and the probability of surviving fibers increases. The degradation of the UFS may also be attributed to fiber degradation.

Based on the discussion above, bonding and debonding of the fiber/matrix phases completely changes the composite fracture behavior. As is proven by EELS analysis, silicon atoms, likely from the SiC phase, diffused into the PyC phase and consequently caused the PyC phase to disappear, which was significant at lower irradiation temperatures. Such inter-diffusion between the SiC and carbon phases was reported for SiC/SiC composite ions irradiated at 300°C [25]. Inter-diffusion among phase boundaries was studied not only for the SiC/PyC interphase [25] but also for the other material systems [29, 30]. The diffusion rate-controlling mechanisms include cascade mixing [29] and radiation-enhanced diffusion [30]. Regardless of the controlling mechanism, it is expected that increasing the interphase thickness may help to preserve the interphase under high-dose irradiation conditions. Regarding the debonding mechanism, an ion irradiation study by Kondo et al. [25] found that differential swelling of HNS fibers and the SiC matrix at 300°C caused the interfacial debonding. This also explains the interfacial debonding at 319°C in this study.

After irradiation at 629°C case, microscale local debonding was found at all the multi-layer PyC phases, which indicates differential dimensional stability between SiC and PyC rather than between fiber and matrix. Unfortunately, the dimensional changes in the PyC phase in SiC/SiC composites under irradiation were not measured because of the experimental difficulty. In

addition, it is difficult to predict dimensional stability because swelling of PyC is highly dependent on material qualities such as density, pore structure, and crystallinity [31, 32]. Moreover, inter-diffusion between PyC and SiC may also affect PyC swelling. In fact, macroscopic properties of PyC phase irradiated to high doses are poorly understood, although the microstructural changes due to intense neutron or ion irradiation have been investigated using TEM [19, 25, 33-35]. The challenge is to achieve adequate fiber/matrix interfacial bonding strength [36] and friction force [23] up to high radiation doses to retain the composite mechanical properties. Modification of the interface design is essential for the development of irradiation-resistant SiC/SiC composites. The design options include changes in the interphase thickness, the interphase material, and the fiber type. New interphase development is reported elsewhere [37], although the irradiation resistance has not yet been proved.

The carbon phase was also not stable in the HNS fiber, as shown in Fig. 8. It is thought that inter-diffusion between the SiC and carbon phases operated like a PyC/SiC multi-layer interphase. The smooth fiber surface after irradiation in Fig. 3 indicates reduction of the fiber fracture energy based on a semi-empirical relationship between the fiber strength and the fracture mirror of the fiber [23]. However, the strength of the fiber itself could not be determined or estimated from the flexural strength because of the complex stress state. If the strength degradation of the fiber is severe, that explains the degradation in UFS, since the statistics for fiber strength determine the ultimate strength of the SiC/SiC composites [38].

In contrast to the interphase and the fiber, there was no indication of strength degradation in the monolithic CVD SiC. The swelling saturated at ~100 dpa, and there was no significant degradation of the Young's modulus by irradiation. Moreover, strength degradation is not expected in CVD SiC with limited cavity sizes and numbers. The strength degradation was only

20% for CVD SiC irradiated at 1500°C to 9.7 dpa [39], and a significant number of voids were formed within grains and along grain boundaries [40]. The current study found formation of cavities at very low temperatures of 534 and 629°C. The lowest void formation temperature for neutron-irradiated SiC was reported to be 1130±85°C [40], at which silicon vacancies with a migration energy of 2.35 eV [41] were effectively mobile. Since irradiation temperatures of 534 and 629°C are anomalously low for void formation, it is possible that transmutation elements such as helium contributed to cavity formation [42]. In this study, a total helium production of ~250 ppm in SiC is expected based on a calculation of transmutation [43].

In summary, this study points out the challenges in developing SiC/SiC composites for high-dose radiation environments, mainly because of the loss of functionality of the fiber/matrix interphase under irradiation. Further efforts are essential to advance the development of irradiation-tolerant SiC/SiC composite materials by modifying the design of the fiber/matrix interface.

Conclusions

Irradiation at 319°C to 92 dpa and at 629°C to 99 dpa significantly degraded the PLS and UFS of CVI SiC/SiC composites with HNS fiber coated with a multi-layer PyC-SiC interphase. In addition, irradiation at 319°C and at 629°C changed the quasi-ductile fracture behavior of nonirradiated material to brittle fracture and to failure with larger fiber pullout, respectively. These changes in the fracture behavior were respectively explained by strengthening of fiber/matrix interfacial bonding and weakened bonding, based on electron microscopy evaluations of PyC phase. This study stresses the need for development of fiber/matrix interphases that are irradiation-tolerant up to high neutron doses to improve the irradiation resistance of SiC/SiC composites. The fiber microstructure also underwent modification: the

number density of carbon impurity phases at grain pockets was obviously reduced. The positive aspects of the high-dose irradiation resistance of the SiC/SiC composite and monolithic CVD SiC were saturations of swelling and changes in the dynamic Young's modulus from a few dpa. Moreover, the CVI SiC matrix and CVD SiC exhibited ignorable cavity swelling at 534°C to 105 dpa and at 629°C to 99 dpa.

Acknowledgments

This research was sponsored by the Office of Fusion Energy Sciences, US Department of Energy, and Japan Atomic Energy Agency (currently National Institutes for Quantum and Radiological Science and Technology) under contracts DE-AC05-00OR22725 and NFE-10-02779, respectively, with UT-Battelle, LLC. A portion of this research used resources at the High Flux Isotope Reactor, a DOE Office of Science User Facility operated by Oak Ridge National Laboratory. The authors wish to thank Anne A. Campbell at Oak Ridge National Laboratory for valuable comments on this manuscript.

References

[1] C. Wong, S. Malang, M. Sawan, M. Dagher, S. Smolentsev, B. Merrill, M. Youssef, S. Reyes, D.K. Sze, N.B. Morley, An overview of dual coolant Pb–17Li breeder first wall and blanket concept development for the US ITER-TBM design, Fusion Engineering and Design 81(1) (2006) 461-467.
[2] P. Norajitra, L. Bühler, U. Fischer, S. Gordeev, S. Malang, G. Reimann, Conceptual design of the dual-coolant blanket in the frame of the EU power plant conceptual study, Fusion engineering and design 69(1) (2003) 669-673.
[3] S. Nishio, S. Ueda, I. Aoki, R. Kurihara, T. Kuroda, H. Miura, T. Kunugi, Y. Seki, T. Nagashima, M. Ohta, Improved tokamak concept focusing on easy maintenance, Fusion engineering and design 41(1) (1998) 357-364.
[4] C. Deck, G. Jacobsen, J. Sheeder, O. Gutierrez, J. Zhang, J. Stone, H. Khalifa, C. Back, Characterization of SiC–SiC composites for accident tolerant fuel cladding, Journal of Nuclear Materials 466 (2015) 667-681.

[5] K. Yueh, K.A. Terrani, Silicon carbide composite for light water reactor fuel assembly applications, Journal of Nuclear Materials 448(1) (2014) 380-388.
[6] D. Kim, H.-G. Lee, J.Y. Park, W.-J. Kim, Fabrication and measurement of hoop strength of SiC triplex tube for nuclear fuel cladding applications, Journal of Nuclear Materials 458 (2015) 29-36.
[7] C. Sauder, Ceramic matrix composites: nuclear applications, Ceramic Matrix Composites: Materials, Modeling and Technology (2014) 609-646.
[8] K. Fitzgerald, D. Shepherd, Review of SiC f/SiC m corrosion, erosion and erosion-corrosion in high temperature helium relevant to GFR conditions, Journal of Nuclear Materials (2017).
[9] J. Braun, C. Guéneau, T. Alpettaz, C. Sauder, E. Brackx, R. Domenger, S. Gossé, F. Balbaud-Célérier, Chemical compatibility between UO 2 fuel and SiC cladding for LWRs. Application to ATF (Accident-Tolerant Fuels), Journal of Nuclear Materials 487 (2017) 380-395.
[10] N.M. George, K. Terrani, J. Powers, A. Worrall, I. Maldonado, Neutronic analysis of candidate accident-tolerant cladding concepts in pressurized water reactors, Annals of Nuclear Energy 75 (2015) 703-712.
[11] N.P. Bansal, Handbook of ceramic composites, Springer Science & Business Media2006.
[12] A. Kohyama, “Inspire” Project for R&D of Sic/Sic Fuel Cladding by Nite Method, Ceramics for Environmental and Energy Applications II: Ceramic Transactions, Volume 246 (2014) 99-107.
[13] S.J. Zinkle, G. Was, Materials challenges in nuclear energy, Acta Materialia 61(3) (2013) 735-758.
[14] T. Yano, H. Miyazaki, M. Akiyoshi, T. Iseki, X-ray diffractometry and high-resolution electron microscopy of neutron-irradiated SiC to a fluence of 1.9× 10 27 n/m 2, Journal of nuclear materials 253(1) (1998) 78-86.
[15] T. Yano, M. Akiyoshi, K. Ichikawa, Y. Tachi, T. Iseki, Physical property change of heavily neutron-irradiated Si 3 N 4 and SiC by thermal annealing, Journal of nuclear materials 289(1) (2001) 102-109.
[16] T. Yano, T. Suzuki, T. Maruyama, T. Iseki, Microstructure and annealing behavior of heavily neutron-irradiated β-SiC, Journal of Nuclear Materials 155 (1988) 311-314.
[17] G. Newsome, L.L. Snead, T. Hinoki, Y. Katoh, D. Peters, Evaluation of neutron irradiated silicon carbide and silicon carbide composites, Journal of Nuclear Materials 371(1) (2007) 76-89.
[18] Y. Katoh, T. Nozawa, L.L. Snead, K. Ozawa, H. Tanigawa, Stability of SiC and its composites at high neutron fluence, Journal of Nuclear Materials 417(1) (2011) 400-405.
[19] A.G. Perez-Bergquist, T. Nozawa, C. Shih, K.J. Leonard, L.L. Snead, Y. Katoh, High dose neutron irradiation of Hi-Nicalon Type S silicon carbide composites, Part 1: Microstructural evaluations, Journal of Nuclear Materials 462 (2015) 443-449.
[20] Y. Katoh, T. Nozawa, C. Shih, K. Ozawa, T. Koyanagi, W. Porter, L.L. Snead, High-dose neutron irradiation of Hi-Nicalon Type S silicon carbide composites. Part 2: Mechanical and physical properties, Journal of Nuclear Materials 462 (2015) 450-457.
[21] R.R. Naslain, The design of the fibre-matrix interfacial zone in ceramic matrix composites, Composites Part A: Applied Science and Manufacturing 29(9) (1998) 1145-1155.
[22] A.A. Campbell, W.D. Porter, Y. Katoh, L.L. Snead, Method for analyzing passive silicon carbide thermometry with a continuous dilatometer to determine irradiation temperature, Nuclear Instruments and Methods in Physics Research Section B: Beam Interactions with Materials and Atoms 370 (2016) 49-58.
[23] A. Evans, F. Zok, The physics and mechanics of fibre-reinforced brittle matrix composites, Journal of Materials Science 29(15) (1994) 3857-3896.
[24] L. Snead, D. Steiner, S. Zinkle, Measurement of the effect of radiation damage to ceramic composite interfacial strength, Journal of nuclear materials 191 (1992) 566-570.
[25] S. Kondo, T. Hinoki, M. Nonaka, K. Ozawa, Irradiation-induced shrinkage of highly crystalline SiC fibers, Acta Materialia 83 (2015) 1-9.

[26] W. Zhou, M.D. Kapetanakis, M.P. Prange, S.T. Pantelides, S.J. Pennycook, J.-C. Idrobo, Direct determination of the chemical bonding of individual impurities in graphene, Physical review letters 109(20) (2012) 206803.
[27] B. Budiansky, J.W. Hutchinson, A.G. Evans, Matrix fracture in fiber-reinforced ceramics, Journal of the Mechanics and Physics of Solids 34(2) (1986) 167-189.
[28] M. Sutcu, W. Hillig, The effect of fiber-matrix debond energy on the matrix cracking strength and the debond shear strength, Acta metallurgica et materialia 38(12) (1990) 2653-2662.
[29] Y.T. Cheng, M. Van Rossum, M.A. Nicolet, W. Johnson, Influence of chemical driving forces in ion mixing of metallic bilayers, Applied Physics Letters 45(2) (1984) 185-187.
[30] F.r. Ding, R. Averback, H. Hahn, Radiation-enhanced diffusion in Ni/Zr diffusion couples, Journal of applied physics 64(4) (1988) 1785-1790.
[31] Y.S. Virgil'ev, I. Lebedev, Effect of neutron irradiation on properties of glassy carbon, Inorganic materials 38(7) (2002) 668-673.
[32] J. Kaae, The mechanical behavior of BISO-coated fuel particles during irradiation. Part I: Analysis of stresses and strains generated in the coating of a BISO fuel particle during irradiation, Nuclear Technology 35(2) (1977) 359-367.
[33] H. Kishimoto, K. Ozawa, O. Hashitomi, A. Kohyama, Microstructural evolution analysis of NITE SiC/SiC composite using TEM examination and dual-ion irradiation, Journal of Nuclear Materials 367 (2007) 748-752.
[34] T. Duh, K. Yin, J. Yan, P. Fang, C. Chen, J. Kai, F. Chen, Y. Katoh, A. Kohyama, Study of helium bubble formation in SiCf/PyC/β-SiC composites by dual-beam irradiation, Journal of nuclear materials 329 (2004) 518-523.
[35] T. Taguchi, N. Igawa, S. Miwa, E. Wakai, S. Jitsukawa, L. Snead, A. Hasegawa, Effect of displacement damage up to 50dpa on microstructural development in SiC/SiC composites, Journal of Nuclear Materials 367 (2007) 698-702.
[36] S. Pompidou, J. Lamon, Analysis of crack deviation in ceramic matrix composites and multilayers based on the Cook and Gordon mechanism, Composites science and technology 67(10) (2007) 2052-2060.
[37] M. Li, X. Zhou, H. Yang, S. Du, Q. Huang, The critical issues of SiC materials for future nuclear systems, Scripta Materialia (2017).
[38] W.A. Curtin, Theory of Mechanical Properties of Ceramic-Matrix Composites, Journal of the American Ceramic Society 74(11) (1991) 2837-2845.
[39] S. Kondo, Y. Katoh, L.L. Snead, Concentric ring on ring test for unirradiated and irradiated miniature SiC specimens, Journal of Nuclear Materials 417(1) (2011) 406-410.
[40] S. Kondo, Y. Katoh, L.L. Snead, Microstructural defects in SiC neutron irradiated at very high temperatures, Journal of Nuclear Materials 382(2) (2008) 160-169.
[41] F. Gao, W.J. Weber, M. Posselt, V. Belko, Atomistic study of intrinsic defect migration in 3C-SiC, Physical Review B 69(24) (2004) 245205.
[42] H. Trinkaus, B. Singh, Helium accumulation in metals during irradiation–where do we stand?, Journal of Nuclear Materials 323(2) (2003) 229-242.
[43] H.L. Heinisch, L.R. Greenwood, W.J. Weber, R.E. Williford, Displacement damage in silicon carbide irradiated in fission reactors, Journal of nuclear materials 327(2) (2004) 175-181.